Semi-annual Technical Report
for the Period 1/1/71 - 6/30/71

Conduction Mechanisms in Thick Film Microcircuits

Grant Number: DAHC15-70-G7

ARPA Order No.: 1642

Grantee: Purdue Research Foundation

Principal Investigator: R.W. Vest
(317) 494-4445

Effective Date of Grant: 7/1/70

Grant Expiration Date: 6/30/73

Amount of Grant: $112,458

August 1, 1971

Forward

The research described in this report constitutes the second six months effort under a grant from the Advanced Research Projects Agency, Department of Defense under the technical cognizance of Dr. Norman Tallan, Aerospace Research Laboratories, United States Air Force. The research was conducted in the Turner Laboratory for Electroceramics, School of Electrical Engineering and School of Materials Science and Metallurgical Engineering, Purdue University, Lafayette, Indiana 47907, under the direction of Professor R.W. Vest. Contributing to the project were Visiting Assistant Professor G.L. Fuller, Mr. D.J. Deputy, Mr. J.L. Wright, and Mr. G.J. Zeeman.

Abstract

Specifications are developed to define "good" resistors and conductors for this project. The design and performance of a laboratory scale three roll dispersing mill is described. The contact resistance between two single crystals of RuO_2 in the presence of glass was measured as a function of temperature and thermal history. After formation of a stable contact during the first firing the contact resistance was observed to be large compared to the crystal resistance, to have a lower TCR, and to increase with repeated firings; models are proposed to explain these results. The coefficient of linear thermal expansion was measured for alloys in the Ag-Pd and Au-Pt systems; the results were correlated with the respective phase diagrams.

TABLE OF CONTENTS

LIST OF FIGURES

LIST OF TABLES

I. Introduction

A. Project Goals and Plans

The current status of thick film technology as applied to conductive and resistive formulations is largely the result of empirical developments. The development of new materials as well as the improvement of existing systems have been hindered by an inadequate understanding of the mechanisms by which electric charge is transported in thick film resistors and conductors.

Any model for conduction in thick film microcircuits must explain the fact that the temperature coefficient of resistance (TCR) of a resistor is much lower than the TCR of any of the individual ingredients from which it was made. Several possible approaches to explaining this "TCR anomaly" which are being explored in this project are:

1. Changes in contact resistance between adjacent particles due to thermal stresses,
2. Changes in the intrinsic properties of the conductive material during processing,
3. Formation of new phases which contribute to the conduction,
4. Size effects which change the intrinsic properties of the conductive,
5. Changes in the geometry factor with temperature.

Published work concerning these possible mechanisms was discussed in the first report on this project [1].

The primary problem in reaching an understanding of typical industrially processed thick film resistor and conductor systems is the complexity of the total manufacturing operation. The large number of variables which influence the value of the resistor make it extremely difficult to purposely change one variable and be certain that some other variable is not changing unexpectedly and completely distorting the meaning of the experimental data. In particular, many resistor systems have small amounts of ingredients added because experience has shown that they improve TCR, stability, etc. From the standpoint of scientific understanding, however, they only cause confusion.

It is felt that the only way to reach an understanding of thick film resistors and conductors is to first perform experiments with the basic ingredient materials and to limit the variety of experimental samples to those that are as conceptually simple and easy to define as possible. This has been the procedure followed in the initial phase of this project in an attempt to identify the important material properties and processing variables, and to determine their influence individually on system performance.

The primary thrust of the experimental program is to relate the electrical properties of the thick films to the material properties and processing conditions through microstructure. The materials properties to be correlated are: resistivity; temperature coefficient of resistivity; coefficient of thermal expansion; interfacial energy; particle shape, size, and size distribution; and chemical reactivity with other constituents. The processing condi-

tions to be correlated are time, temperature, and atmosphere during firing. The morphological studies of the fired films will involve the identification of the conducting phases, their size, shape, distribution, composition, and interaction. The thick film resistor portion of this project will use ruthenium dioxide conductive, $PbO-B_2O_3-SiO_2$ glass, and 96% Al_2O_3 substrate as the basic test system to relate material properties to microstructure and system performance. The investigation of thick film conductives involves the study of the noble metals-gold, silver, platinum, and palladium, as well as alloys among them.

Based on the experimental results, suitable theories of the electrical properties of heterogeneous systems will be envoked to correlate the data and to aid in the development of phenomonological models to inter-relate the various material properties with system performance.

B. Resistor and Conductor Specifications

In order to achieve the goals of this research program it will be necessary to characterize the microstructure of good resistors and conductors. The implicit assumption in this requirement is that "good" resistors and conductors can be defined. The desire to keep the test systems as simple as possible introduces a rather severe boundary condition; if we knew at this point in time how to make thick film microcircuits satisfy the most rigid specifications when fabricated from simple systems there would be no need to continue the research. Therefore, compromises with performance were made consistent

with what we believe is possible to achieve. Military specifications have been followed as much as possible so that all test procedures are adequately defined.

1. Electrical Specifications

1.1 Temperature Coefficient of Resistance

The TCR of a resistor must be less than ± 300 ppm/°C from -55° to 125°C in accordance with paragraph 3.16, MIL-R 55188(EL) for a Type U resistor.

1.2 Power Rating

The power rating of a resistor must satisfy the load life requirements of 1.3. A nominal figure is 30 watts per square inch of resistor area.

1.3 Load Life

The load life of a resistor must be such that the change in resistance is less than ± (1% + 0.05Ω) after 1000 hours operation at the rated wattage at 125°C in accordance with paragraph 3.18, MIL-R-10509F.

1.4 Voltage Rating

The continuous operating D.C. or 60Hz RMS voltage (E) of a resistor is given by $E = \sqrt{PR}$,

where

P = power rating

R = nominal resistance

in accordance with paragraph 3.6, MIL-R-10509F.

1.5 Short-time Overload

The change in resistance for a resistor must be less than ± (0.5% + 0.05Ω) after application of a voltage equal to 2.5E for 5 seconds in accordance with paragraph 3.11, MIL-R-10509F and paragraph 3.9, MIL-R-55188(EL).

1.6 Low Temperature Exposure

The change in resistance for a resistor must be less than ± (0.5% + 0.05Ω) after exposure to -65°C for 24 hours in accordance with paragraph 3.18, MIL-R-55188(EL).

1.7 Temperature Cycling

The change in resistance for a resistor must be less than ± (1.0% + 0.05Ω) after five (5) cycles of -65° to 175°C in accordance with paragraph 3.17, MIL-R-55188(EL).

1.8 Current Noise

When tested at voltage E the noise in a resistor must not exceed the following limits in accordance with paragraph 3.12, MIL-R-55188(EL).

Resistance Range (Ω)	Noise (μv/v)
10 - 30,000	0.3
30,000 - 70,000	0.4
70,000 - 100,000	0.5

1.9 Moisture Resistance

The change in resistance for a resistor must be less than ± (0.5% + 0.05Ω) after ten cycles in accordance with paragraph 3.21, MIL-R-55188(EL).

1.10 Voltage Coefficient of Resistance

The VCR of a resistor must be less than ± 50 ppm/volt/in for voltages up to E when measured in accordance with Method 309, MIL-STD-202C.

1.11 Resistance to Soldering Heat

The change in resistance for a resistor must be less than ± (0.5% + 0.05Ω) after exposure to 230°C for 1 hour.

1.12 Resistivity

The resistivity of a conductor must be less than 0.1 ohm per square for conductive thicknesses less than 0.001 inch.

2. Mechanical Specifications

2.1 Shock

The change in resistance for a resistor must be less than ± (0.1% + 0.05Ω) after being subjected to 30 shocks at 50G's in accordance with paragraph 3.19, MIL-R-55188(EL).

2.2 Vibration

The change in resistance for a resistor must be less than ± (0.1% + 0.05Ω) after being subjected to frequencies between 10 and 2000 Hz at 15G's in accordance with paragraph 3.20, MIL-R-55188(EL).

2.3 Altitude

The change in resistance for a resistor must be less than ± (0.1% + 0.05Ω) after exposure for one hour to a pressure of 0.043 inches of mercury (150,000 feet) in accordance with paragraph 3.22, MIL-R-55188(EL).

2.4 Solderability

A solderable conductive must show 95% coverage with 60% Sn-40%Pb solder when tested in accordance with paragraph 3.19, MIL-R-10509F.

2.5 Adherence

The bond strength for a solderable conductive must be at least 2.0 pounds when tested in accordance with Dupont's test [2] for wire peel adhesion.

II. Experimental

A. Roller Mill

An important aspect of maintaining uniformity in thick-film inks is the uniform dispersion of the inorganic powders in the screening agent. Although paddle wheel types of blenders are often adequate for macro dispersion and for redispersing after settling, experience has shown that they are usually not sufficient for microdispersion (breaking up small agglomerations of powder held together by surface forces). To accomplish a through and presumably uniform dispersion the thick-film industry has for many years used a three-roll mill (shown schematically in Fig. 1.)

Two of the rolls are for mixing; they rotate in opposite directions, and are either positioned to maintain a very small spacing or are held together under spring tension. The surfaces of the two mixing rolls move downward at their point of contact in order to contain the volume of material being mixed. The second roll rotates faster than the first so that there is a shear force between the rolls that improves dispersion over what it would be if both rolls rotated at the same rate; the greater the shear, the better the dispersion. The third roll is called the take-off or transfer roll. It accomplishes the removal of the mixed material from the mill by removing it from the second roll and transferring it to the take off blade that scrapes the ink off the roll. The third roll rotates faster than the second roll to avoid any accumulation of material.

Commercially available three-roll mills which have the features described above are quite expensive, and in addition, require a minimum

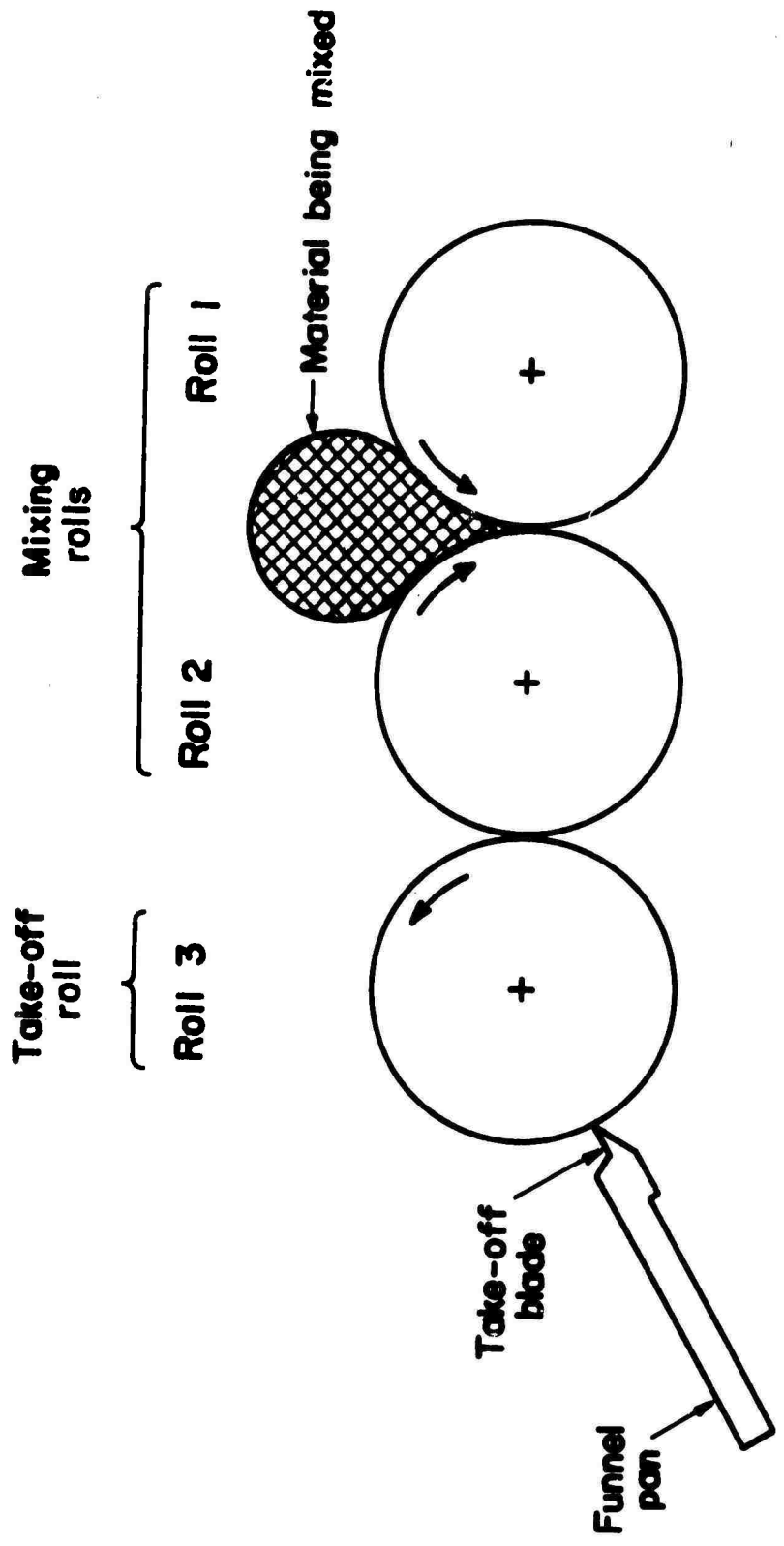

Figure 1. Three Roll Dispersing Mill Schematic

of several hundred ml of formulation for proper operation. To overcome these difficulties, the three-roll mill, shown in Fig. 2, was designed and constructed for laboratory formulation of research inks. Figure 2a shows a dispersing cycle using a silver-palladium conductive formulation, and the take-off cycle is shown in Fig. 2b. The small rolls, 1-1/4 inch diameter X 4 inch long, permit the blending of quantities as small as 5-10 ml and up to about 50 ml, and are made of type 303 stainless steel. This is not an optimum material, but has been adequate for current requirements. The spindles are mounted on modified gimble sleeve bearings that provide desirable run-out while permitting small mis-alignments during adjustment and cleaning. The two outer rolls are mounted in slide blocks that are individually adjusted as shown. The adjustment mechanism uses 1/4-40 threads for micrometer adjustment and is presently rigid, but will eventually incorporate a spring drive that will reduce the possibility of damage to the rolls. The gear train consists of spindle, idler and drive gears, as shown. This design permits the rolls to operate with any spacing from 0 to 0.25 inch (convenient for cleaning), and provides for a ratio of roll rotation of 50:150:300. This combination represents a compromise such that the first roll rotates fast enough to keep a large amount of ink on the mill, the third roll rotates slow enough that the ink will not come off due to centrifical force, and the shear rate between the mixing rolls is sufficiently large. The drive motor is a 5-221 rpm gear motor with electronic speed control that normally operates at 200 rpm. The take-

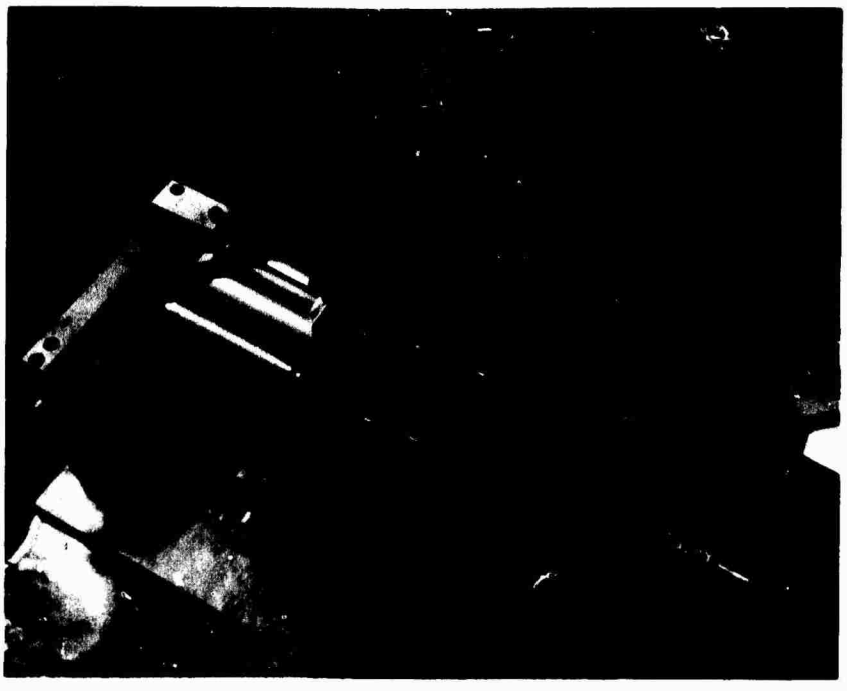

a. Dispersing Cycle

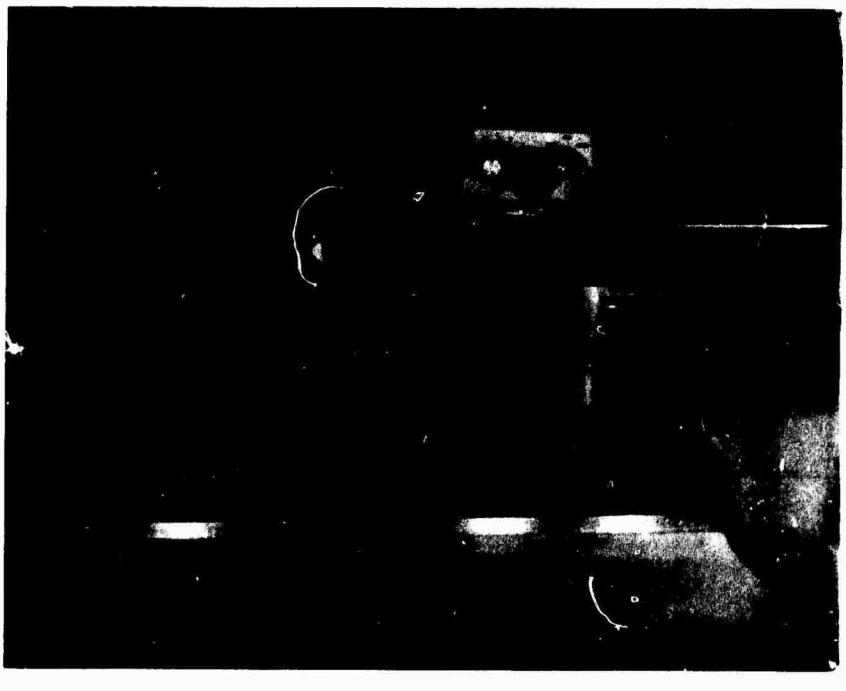

b. Take-off Cycle

Figure 2. Laboratory Three Roll Mill

off blade and funnel pan unit and the retainer blocks between the first and second rolls are made of brass, are free to align to the rolls, and are held in place with spring mechanisms. All spindles and rolls are hollow so that rotating water couplings may be connected to permit variations in the temperature of the rolls, either hotter or colder than ambient.

B. Sample Preparation

1. Noble Metal Alloys

The alloys for thermal expansion measurements were prepared from -325 mesh powders of Ag, Au, Pd, and Pt. The purity level exceeded 99.9% for all four metals. The nominal compositions of the alloys prepared are given in Table I along with the actual compositions. The actual compositions were calculated from measurements of the pycnometric density of the cast alloys. In the Ag-Pd system, which is reported [3] to exhibit complete solid solubility, the compositions were chosen at even spacings with the addition of an alloy at 70% Pd; this is near the composition where both the hardness and tensile strength have maximum values [4]. The choice of compositions in the Au-Pt system was made on the basis of reported intermetallic compounds and a solid solution misability gap [3], and on maxima in the resistivity, tensile strength, and hardness [4].

The cost of the metals and the limited constant temperature region of the furnace used with the dilatometer restricted the sample size to dimensions less than the ASTM minimum requirement

Table I. Alloy Compositions for Thermal Expansion Measurements

Silver - Palladium (weight percent Pd)		Gold - Platinum (weight percent Pt)	
Nominal	Actual	Nominal	Actual
20	20.01	10	10.55
40	40.27	20	19.97
60	60.11	25	24.51
70	69.48	29	28.75
80	79.98	60	59.97
		80	79.96

[5] of a 2 inch X 3/16 inch diameter sample. Trial runs varying the size of wire samples showed that a 1 inch X .065 inch diameter sample exhibited sufficient mechanical stiffness at high temperatures to resist the force of the dilatometer assembly without bending. The final sample size of approximately 0.5 inch by 0.06 inch diameter was determined primarily by problems in the melting operation.

The molds used to form the rods were 3 inch long sections of double bore thermocouple protection tubes. The tubes were 99.9% alumina with a manufactor suggested maximum service temperature of 1950°C. A water and powdered alumina mixture was used to close one end of the tubes. The plugged tubes were dried at 600°-700°C for at least 2 hours. It was found that a 1/4 inch plug was more than sufficient to prevent any leakage of the liquid metal.

An effective packing of the powder was hampered by the non-uniformity of the approximately elliptical bore in the molds. Tapping the mold while filling seemed to produce a more uniform packing than using a ram smaller than the bore size. Ideally, a ram with the same approximate cross-sectional shape and size similar of the bore would allow a more efficient packing but the lack of shape uniformity, through the mold and from mold to mold, eliminated the practicality of this possibility. Insufficient packing pressure caused a large amount of gas entrapment in the melt. Although thermal expansion should be independent of porosity, a comparison of two Pd rods, one of desired quality and the other cast without reducing the amount of entrapped gases, showed a 10% descrepancy in their α_m values. The exact cause of this discrepancy was not known, but the need to eliminate the entrapped gases was clear.

The casting apparatus consisted of two separate and sealed chambers; a heating chamber and a sample chamber. The heating chamber utilized tantalum sheet heating elements in a water cooled shell. The sample chamber was a brass cylinder with a 1 1/8 inch diameter closed end alumina tube protruding into the center of the heating chamber. The temperature was monitored with an optical pyrometer focused on the alumina tube through a observation port in the furnace wall.

Argon atmospheres were maintained in both chambers through-out the sample processing. The argon was purified by passing through a bed of titanium shavings at 800°C before entering the system. An argon purge of both chambers to eliminate other gases lasted 30 minutes, then the flows were decreased to establish a pressure of slightly above atmospheric. The system was heated slowly to allow the residual gases to be carried out of the system by the argon flow and also to prevent thermal shock of the alumina tube.

If a casting operation was carried out with the powders under a pressure of one atmosphere the resultant rod was always found to contain a multitude of blow holes caused by gas entrapment. Increasing time at maximum temperature from 30 minutes to 210 minutes resulted in the formation of several short smooth rods within the curcible. A similar result was obtained when the alloys were cast in vacuum. It was found, however, that the surface tension between the melt and the crucible could be overcome by increasing the pressure above the melt to 1.1 - 1.2 atm. after melting under a reduced pressure.

Based on the above considerations, the following procedure was established. The sample chamber was evacuated to a pressure of 30 torr at 50°C below the solidus curve. The heating was continued to 150°C above the liquidus and the sample held at this temperature for 30 minutes. Before starting to cool the melt, the sample chamber pressure was increased to 1.15 atm. Due to lack of bore uniformity and/or diffusion bonding, the rods had to be broken out of the molds. The ends of the rods were filed flat and the rods were ready for expansion analysis.

The sample rods were placed in a sample holder made of two concentric fused quartz tubes that had a length less than the sample. The inside diameter of the holder was large enough to allow the rod to expand freely. The holder served as a stabilizer to prevent a transverse motion of the measuring rod-sample interface, and the added thermal mass tended to smooth the furnace temperature profile.

2. Crossed Single Crystals of RuO_2

To measure the resistance of a single contact between two small crystals of RuO_2 in the presence of glass, the crystals were each mounted on two 0.005 inch diameter platinum wires bonded to conductive pads on an alumina substrate. One wire on each crystal served for the potential lead and one for the current lead, in a configuration such than the crystals crossed at a point of contact near one end. Thus, the measured resistance was the sum of the contact resistance and single crystal resistances between the potential leads and the point of contact. The 0.005 inch wire was used to mount the crystals in order to provide sufficient rigidity to maintain contact but to allow enough flexibility for the negative coefficient of ther-

mal expansion of the RuO_2 [1] in the c direction, the growth direction of the single crystal rods.

The first sample prepared had a temperature dependence of total sample resistance that was similar to single crystal RuO_2 as measured by the automatic resistance measuring system [1]. However, one of the RuO_2 crystals was found to be hollow and hence higher in resistance, and no method was available to determine accurately the resistance due to only the contact.

To overcome this latter problem a new sample was prepared that was a six lead device instead of only four. Two additional leads were attached to the ends of the crystals beyond the point of contact. These extra leads permitted four terminal resistance measurements of each crystal with the point of contact serving as one potential lead, and allowed for the determination of crystal resistance up to the point of contact. The mounted crystal is shown in Fig. 3. The lead wires were attached to the crystals with Englehard 6082 fluxed platinum paste which was previously discussed and characterized [1].

After the crystals and lead wires were attached, the 0.005 inch platinum mounting wires were bent slightly to create a contact between the crystals. Glass* powder was then mixed with Carbitol (Diethylene Glycol Monobutyl Ether) to form a paste and applied to one side of the region of intersection. Carbitol was chosen because of its slow evaporation rate at room temperature. With glass at the area of contact, the sample was exposed to increasing temperatures from 600° to 800°C and then recycled to 800°C.

---

* Lead-borosilicate glass characterized in reference [1].

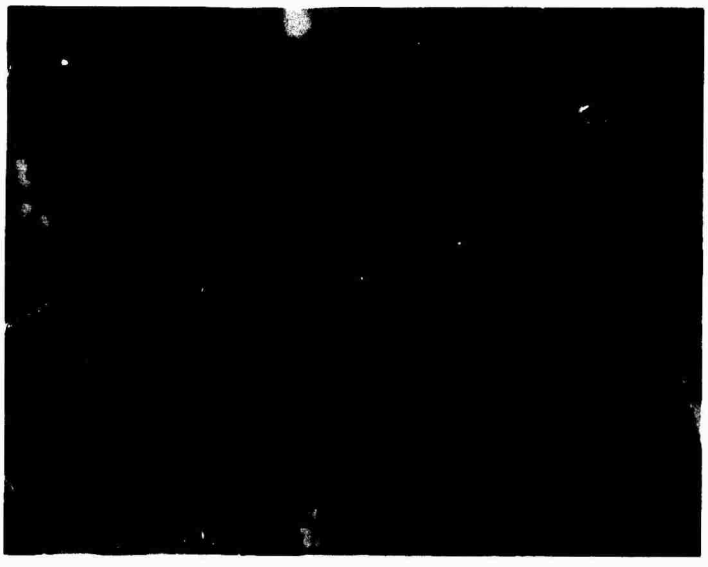

Figure 3. Crossed Single Crystals of RuO_2 (40X)

III. Results and Discussion

A. Crossed Single Crystals of RuO_2

The thermal history of the crossed single crystals of RuO_2 is given in Table II. The sample resistance was continuously monitored to the maximum temperature with the automatic resistance measuring system [1] throughout each firing cycle. Fig. 4a shows the resistance - time behavior during the early portion of the first firing cycle (600°C maximum temperature) for the temperature - time cycle shown in Fig. 4b. The sample resistance was unstable in the early portion of the cycle as might be expected for the "point" contact of two hard surfaces. The resistance oscillated from about 7 to 30Ω often with frequencies up to the response limit of the chart recorder (5Hz). At approximately the softening point of the glass (480°C) the resistance decreased almost an order to magnitude, and remained low and relatively noise-free for the remainder of the cycle.

A visual observation of the sample after Cycle A showed that the glass had sintered with entrapped air bubbles as previously discussed [1], and showed slight signs of wetting to the crystals. Thus, the glass seemed to be rigidly attached to the two crystals but the amount of glass at the point of contact could not be determined. Judging by the limited amount of wetting observed on the top of the sample it seems unreasonable that any glass was present in the interface of the crystals.

Table II. Thermal History of Crossed Single Crystals of RuO_2

Firing Cycle ($30^{\circ}C$/min)	Maximum Temperature ($^{\circ}C$)	Measurement Cycle	TCR (ppm/C°)	Comments
012671A	600			Add glass before cycle
		A	3770	
012871A	700			
		B	2980	
020371A	800			
		C	3260	
020471A	800			
		D	2750	Removed the sample from the furnace to obtain crystal resistance. Sample resistance became erratic.
021271A	800			Add glass before cycle. Sample resistance became infinite at the completion of the firing cycle.
021271B	800			Add glass before cycle. Heating and cooling rate of $60^{\circ}C$/min near $800^{\circ}C$
		E	3400-3800	Sample resistance was not stable versus temperature.

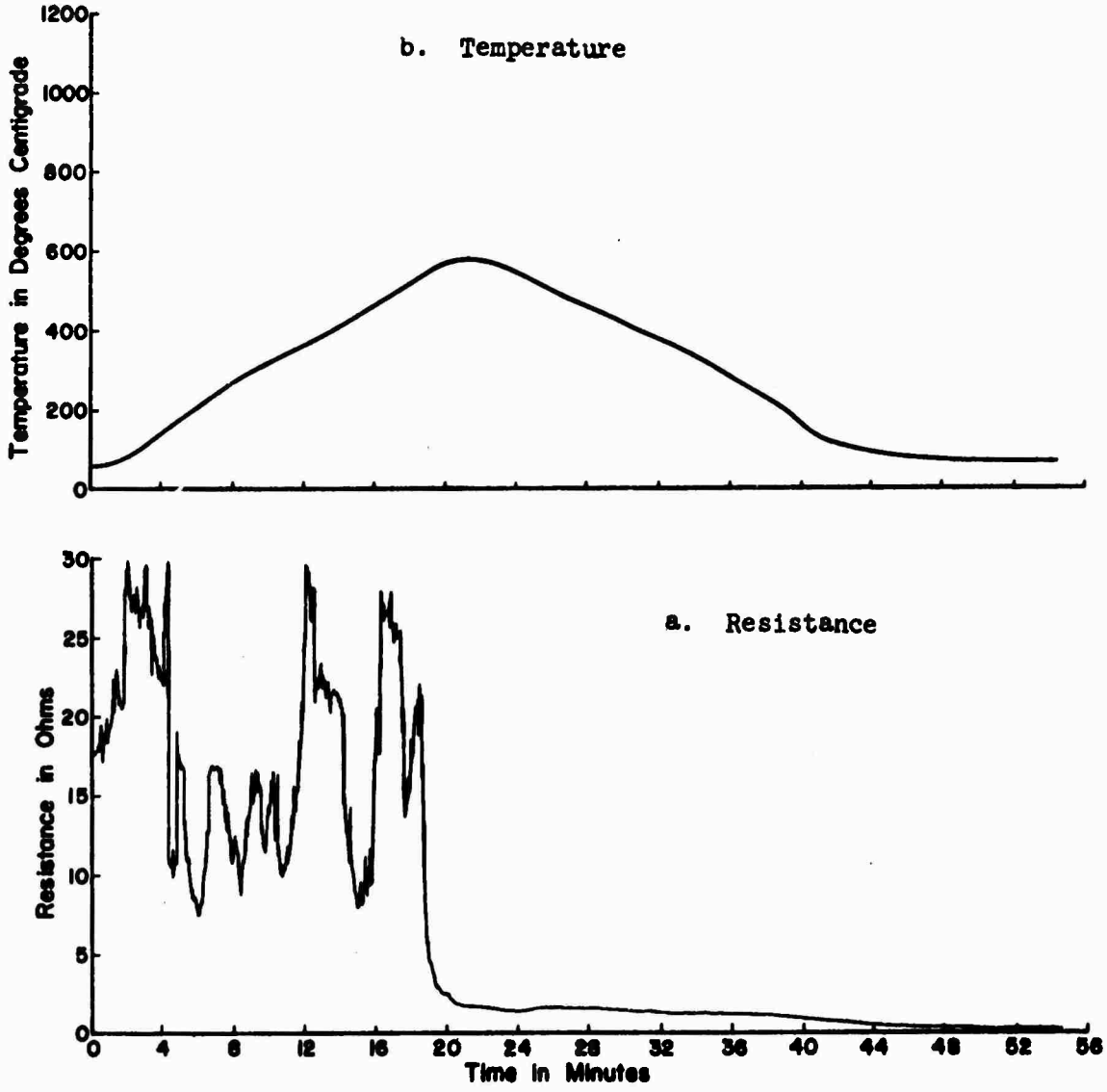

Figure 4. Initial Firing of Crossed Single Crystals of RuO_2

Upon reheating the sample for the next and all subsequent firing cycles, the sample resistance remained well behaved up to about the softening temperature of the glass (as shown in Fig. 5.) At this point the sample resistance increased several fold over a temperature range of about 50°C, and then decreased to near the original value. Above 600-700°C the resistance was nearly constant with some low frequency erratic behavior apparently due to the fact that the viscosity of the glass had a damping effect on crystal motion.

For all cycles the sample resistance was accurately measured from 70° to 250°C with a potentiometer utilizing the four probes discussed in Section IIC2; these results are shown in Fig. 6, and the TCR's (extrapolated to room temperature) of the contact resistance are given in Table II. The sum of the crystal resistance is about 0.01Ω and 0.02Ω at 80° and 250°C respectively, so the measured resistance is almost entirely contact resistance. With the exception of the erratic behavior observed during Cycle E, the contact resistance at any temperature increased by a factor of two during the life of the sample.

The sample was removed from the firing facility after measurement cycle D to determine the room temperature resistivity of the crystals. It was observed that although the crystal resistance measurements were repeatable, the contact resistance was not. A visual observation failed to clearly show the presence of any glass near the point of contact although the observation after the 700°C firing cycle (Cycle B) showed that the glass had completely wet the RuO_2 and had completely encircled the point of contact. Therefore, it was assumed that insufficient glass was present at the point of contact to main-

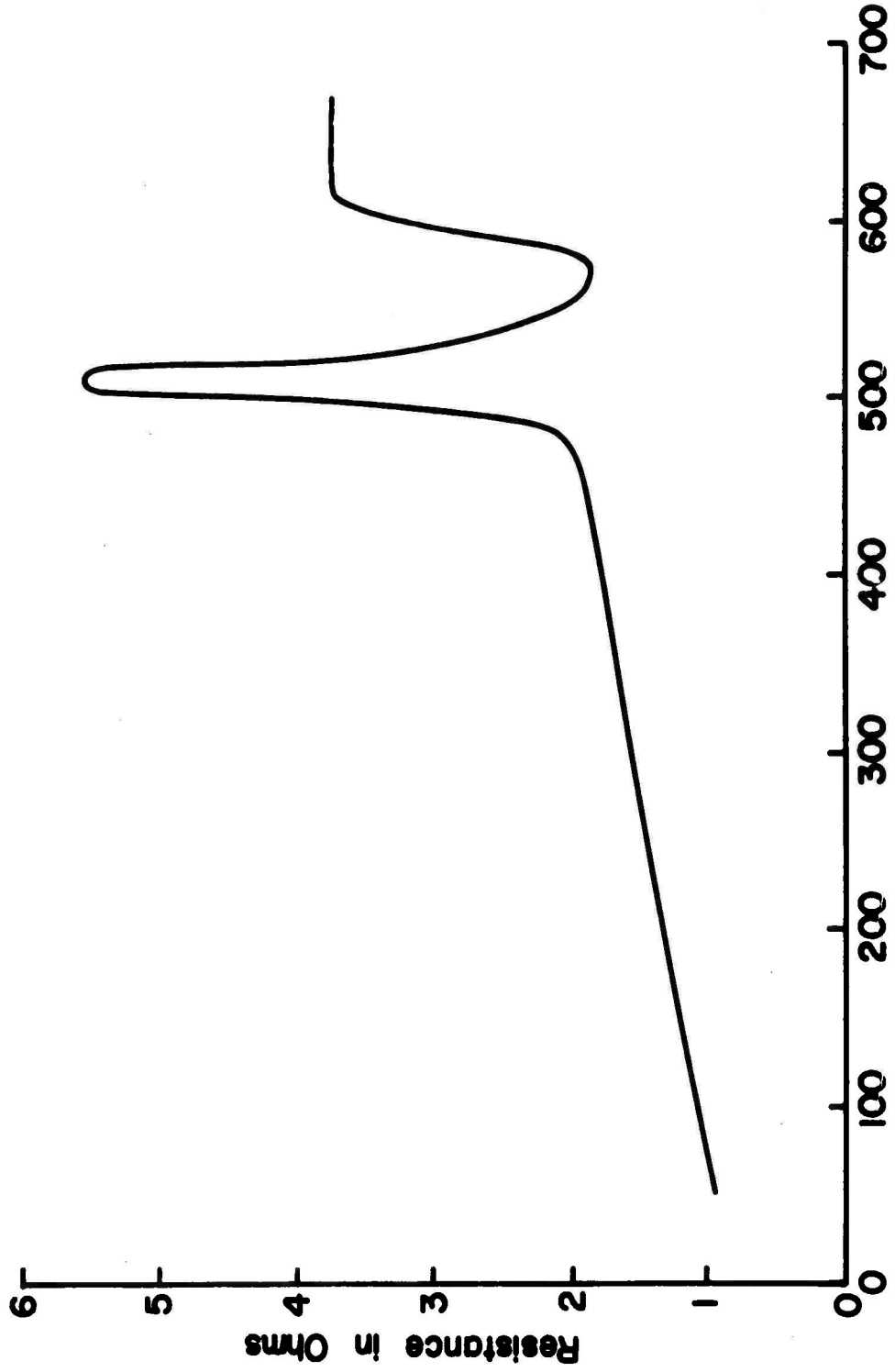

Figure 5. Resistance of Crossed Single Crystals of RuO_2 During Refire

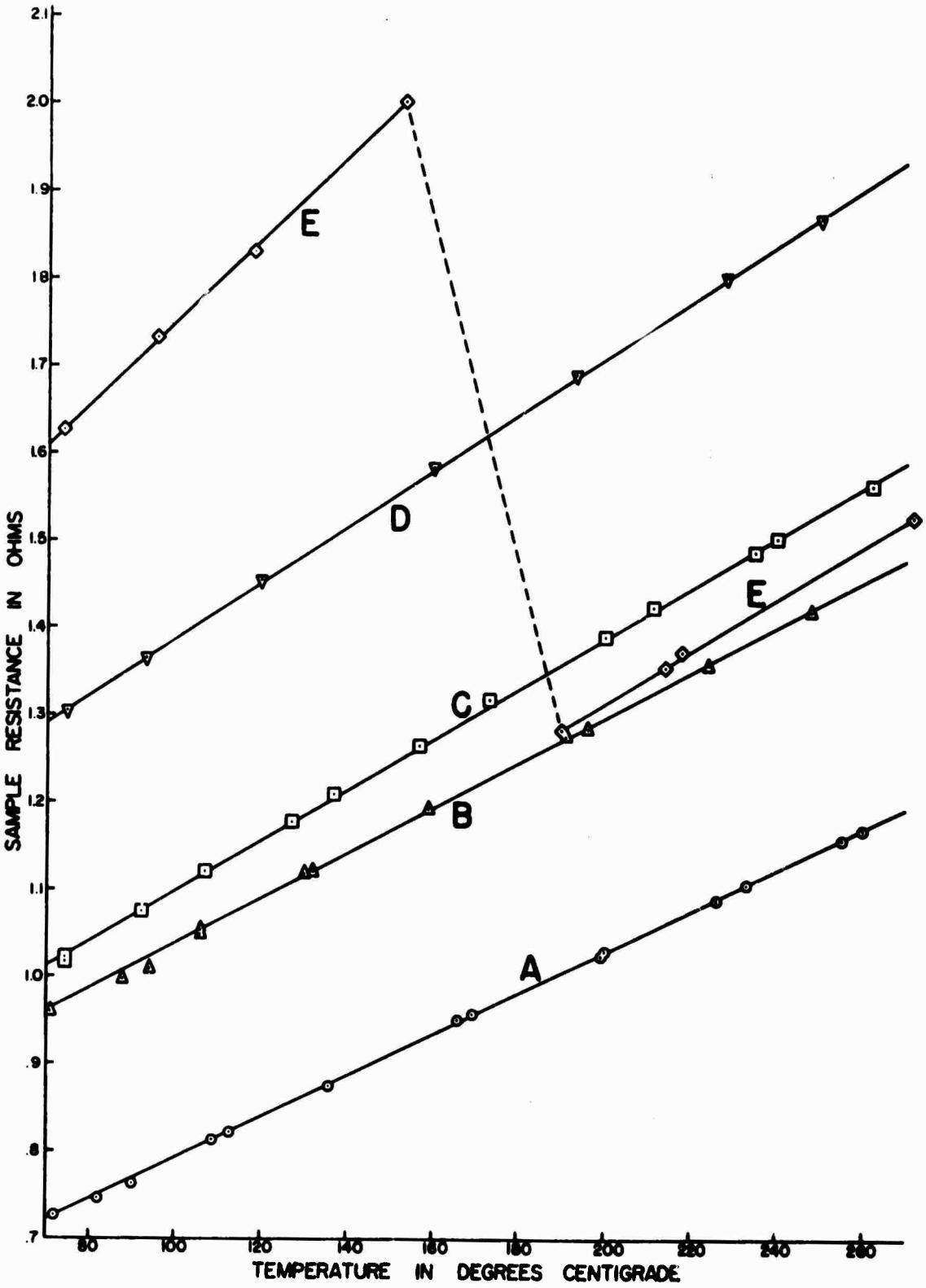

Figure 6 Temperature and Thermal History Dependence of the Resistance of Crossed Single Crystals of RuO_2.

tain the bond under the stress resulting from the negative thermal expansion coefficient of RuO_2. More glass was added for additional exposures to 800°C but some additional erratic behavior was noted as summarized in Table II.

Fig. 7 compares the normalized contact resistance to the resistance of single crystal RuO_2. Although there was a monotonic increase in contact resistance, the TCR of the contact resistance, as indicated by the slopes of the lines, was more random. However, all contact resistances have significantly smaller slopes than single crystal RuO_2, the minimum slope corresponding to almost half the TCR.

The important results of the crossed crystal experiment were: (1) the large contact resistance (about 1Ω compared to $.01\Omega$ for the crystal resistance); (2) the relative values of TCR compared to that of single crystal RuO_2; (3) the increase in resistance with repeated firings to high temperatures; and (4) the dramatic decrease in contact resistance and noise which occurred at the softening point of the glass on the first firing cycle.

The 1Ω contact resistance is not difficult to explain: it could have been due to a very small diameter at the point of contact, i.e., constriction resistance. The radius of the contact area can be estimated with the common formula for constriction resistance $R = \frac{\rho}{2\alpha}$, where R is the constriction resistance, ρ is the resistivity of the bulk material and α is the radius. For RuO_2 with a resistivity of about 50 $\mu\Omega$-cm at 70°C, a contact resistance of 1Ω would require that the radius be 0.25 μm. This is within a reasonable range of contact size.

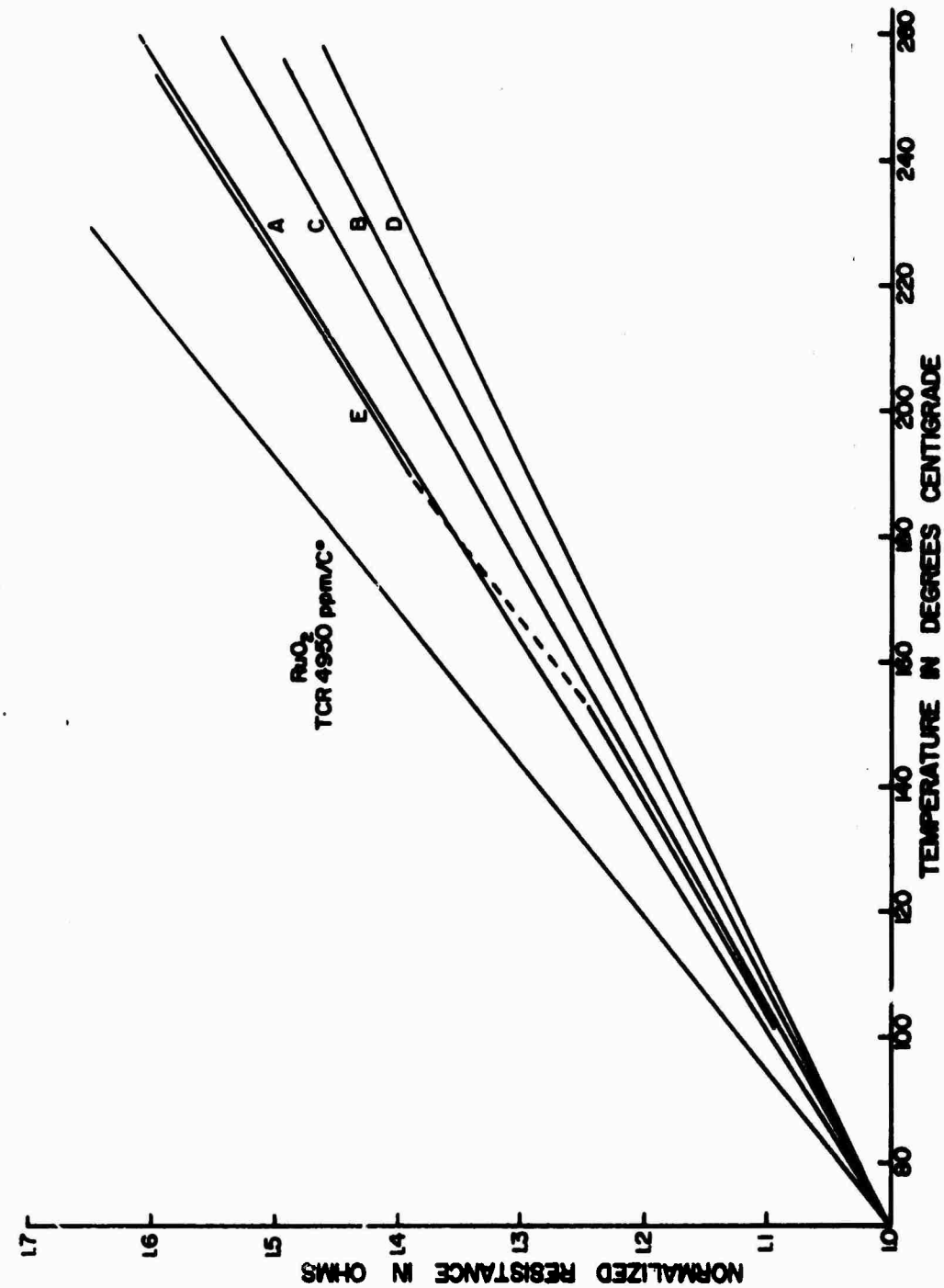

Figure 7. Normalized Resistance as a Function of Temperature for Crossed Single Crystals of RuO_2

The existence of a constriction resistance alone will not explain the lower TCR since the constriction resistance should have the same TCR as the bulk material. To explain this change an additional source of resistance is needed that has a smaller temperature dependence. One possibility is that the resistivity near the surface of the crystal is higher and the TCR lower than for massive single crystal RuO_2 due to increased disorder, and hence electron scattering. This effect could be adequate to explain the lower TCR, but with the glass present there are two additional possibilities.

One possible effect of the glass would involve contact resistance changes due to temperature dependent mechanical strain at the point of contact, i.e., due to differences in thermal expansion between glass and the RuO_2. It is the expansion in the a direction of RuO_2 that must be considered because the c axis is the growth direction of the single crystal rods. This is a mechanism that has been hypothesized for resistors as discussed in the previous report on this project [1]. Comparison of the two thermal expansions shows that the a direction expansion of RuO_2 is almost equal to that of the glass up to about 125°C, and larger than that of the glass at higher temperatures. Thus, without calculating resistance as a function of compressibility, etc., it can be seen that a pressure dependent contact resistance model would not have the correct temperature dependence to explain the almost straight line behavior shown in Fig. 6. The contact resistance could be influenced by this effect, but only to a small degree.

The possibility of tunneling through a thin layer of glass must also be considered. Tunneling resistance can be very dependent on voltage and temperature, and in fact, at least one type of cermet film has been prepared in which voltage dependent tunneling was observed. [6]

However, it is also possible to have a tunneling that is almost independent of temperature and voltage [7-9], depending only on the barrier material, and the magnitude of the potential. The resistance tends to be independent of temperature when the potential across the barrier is small compared to the height of the barrier, and independent of applied voltage for thin barriers. If the potential is sufficiently small (<100mv), the resistance is independent of applied voltage for any barrier thickness. If a barrier thickness of 5-10Å is assumed with impurity enhancement [10] due to RuO_2 dissolved into the thin barrier, the resistivity for tunneling would be approximately $10^{-8}\ \Omega\text{-cm}^2$. Thus, to establish a resistance of 1Ω would require an area of $10^{-8}\ \text{cm}^2$, or a diameter of 1.1μm. It seems unreasonable that an area so large could have a thickness of 5-10Å. Thus, although the temperature (and voltage) dependencies are of the correct form, the resistance values anticipated are too high to be compatible with the observed results.

It is difficult to propose a model which will predict both the increasing resistance and the varying TCR that occurred with repeated firing. The increasing resistance could have easily been due to a decreasing contact area resulting from changes in mechanical strain, but this should be accompanied by a decrease in TCR; the TCR both increased and decreased during the firing cycles. Mechanical effects are important, however, as demonstrated by the fact that the contact resistance increased temporarily at the softening temperature of the glass on every heating cycle. Several other possible effects could lead to a decreasing contact area, but all would be accompanied by no change or, at best, a unidirectional

change in the TCR. The increasing contact resistance strongly suggests that reactive sintering could not have occurred between the two crystals because this mechanism would have decreased the contact resistance for successive cycles.

The large decrease in resistance accompanied by the elimination of contact noise which occurred at the softening point of the glass during the first firing cycle demonstrated that the role of the glass is more than that of a simple binder. Since the quiet contact is formed at a temperature where the viscosity of the glass is still the order of 10^6 poise, no flow, and only limited sintering, could have occurred. Regardless of which of the mechanisms for charge transport across the contact are dominant, it is apparent that it is the interfacial forces between the glass and the RuO_2 which play the dominant role in the formation of the contact.

Based on our results, mechanical stress cannot contribute to the formation of the contact, but this effect does contribute to the resistance of the contact at lower temperatures as demonstrated by the abrupt increase at the softening point on refire (Fig. 5). This behavior is also observed with RuO_2 resistors as shown in Fig. 8. The resistor was made from a mixture of 3% by weight RuO_2 powder and glass powder fired in a recessed area of an alumina substrate as previously described [1]. The decreasing resistance at temperatures above 600°C is due to the conductivity of the glass in parallel with the resistor, but the increase in resistance starting at about 480°C (the softening point of the glass) is characteristic of the resistor. This similarity of the resistor behavior to that of the crossed single crystals lends credence to the extrapolation of results and conclusions from the single contact experiments to a resistor containing a multitude of contacts.

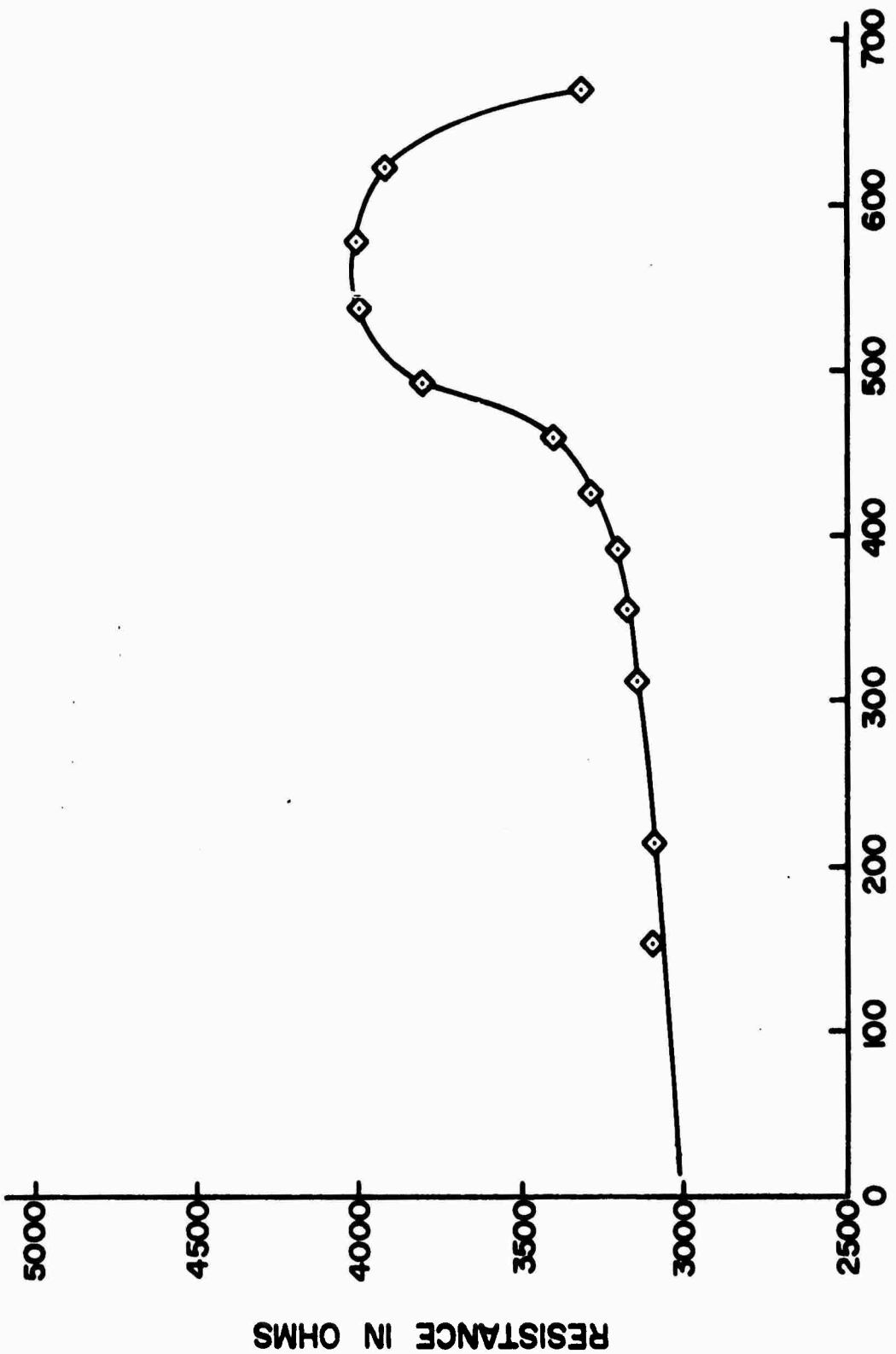

Figure 6. Resistance of an RuO_2 Resistor as a Function of Temperature

B. Thermal Expansion of Noble Metal Alloys

One of the more important parameters for characterizing materials for thick film conductives is the coefficient of linear thermal expansion. This property is needed in order to calculate the mechanical stress present in a conductive so that observed quantities such as resistivity, TCR, and adhesion can be fit to a more complete phenomonological model.

The thermodynamic coefficient of linear thermal expansion is defined as

$$\alpha = \frac{1}{L}\left(\frac{\partial L}{\partial T}\right)_P \tag{1}$$

where the length L is a function of temperature at constant pressure. For practical applications, such as calculation of thermal stresses, the mean coefficient of linear thermal expansion between temperatures T_o and T_1,

$$\alpha_m = \frac{L_1 - L_o}{L_o(T_1 - T_o)} \tag{2}$$

is very useful.

Over a limited temperature range the thermal expansion of most materials can be satisfactorily approximated by a quadratic

$$L = L_o + a(T-T_o) + b(T-T_o)^2. \tag{3}$$

In this case

$$\alpha = \frac{a + 2b(T-T_o)}{L_o + a(T-T_o) + b(T-T_o)^2}, \tag{4}$$

$$\alpha_m = \frac{a + b(T-T_o)}{L_o}, \tag{5}$$

and the relative thermal expansion is

$$\frac{\Delta L}{L_o} = \frac{a(T-T_o) + b(T-T_o)^2}{L_o} \qquad (6)$$

The expansion measurements were made with a fused quartz dilatometer (Model Dilatronic I, Theta Industries, Inc.) utilizing a linear variable differential transformer to detect length changes. The heating rate was 200°C per hour. The data presented in this section were computer fit to Eq. (3) by the least squares method, and α, α_m, and $\Delta L/L_o$ calculated from Eqs. (4-6).

1. Silver - Palladium

The parameters calculated from expansion data over the temperature range 22°-800°C for the various silver-palladium alloys are given in Table III. Fig. 9 shows the relative expansion of the alloys, and Figs. 10 and 11 show the thermodynamic and the mean coefficients of linear thermal expansion at various temperatures. The values of α_m for the pure metals from room temperature to 500°C found in this study are slightly lower than those reported in the literature [11]: 11.7 for palladium versus a reported 12, and 17.8 for silver versus a reported 19. Since the sample size used in this study did not conform to the ASTM standard [5] for use in a quartz dilatometer, this small discrepancy is not surprising. However, comparisons among the alloys should be valid because all samples were of approximately the same size.

The commonly accepted phase diagram for the Ag-Pd system [3] shows complete solid solubility. If this were true, the first order approximation for the coefficient of linear thermal expansion of alloys in the system would be a linear extrapolation between the coefficients of the

Table III

Calculated Parameters for Thermal Expansion of Silver - Palladium Alloys

$$L = L_o + a(T-22^\circ) + b(T-22^\circ)^2$$

weight % Pd	L_o(in)	a(in/°C)	b(in/°C^2)
0	0.568	8.64×10^{-6}	3.05×10^{-9}
20	0.568	7.46×10^{-6}	2.50×10^{-9}
40	0.474	4.98×10^{-6}	2.47×10^{-9}
60	0.518	5.88×10^{-6}	1.79×10^{-9}
70	0.496	5.28×10^{-6}	1.92×10^{-9}
80	0.427	4.53×10^{-6}	1.58×10^{-9}
100	0.533	5.14×10^{-6}	2.29×10^{-9}

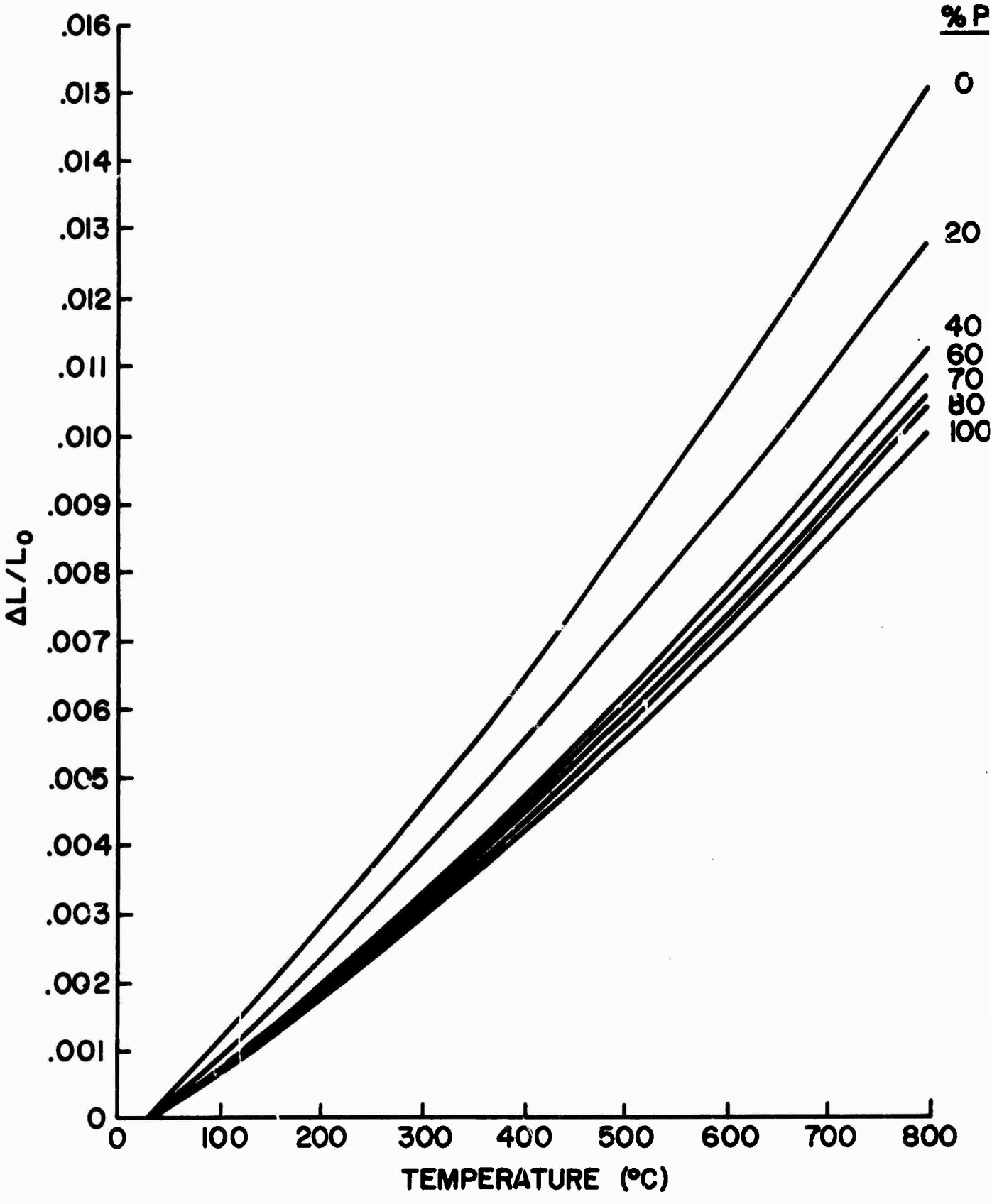

Figure 9. Relative Expansion of Silver-Palladium Alloys

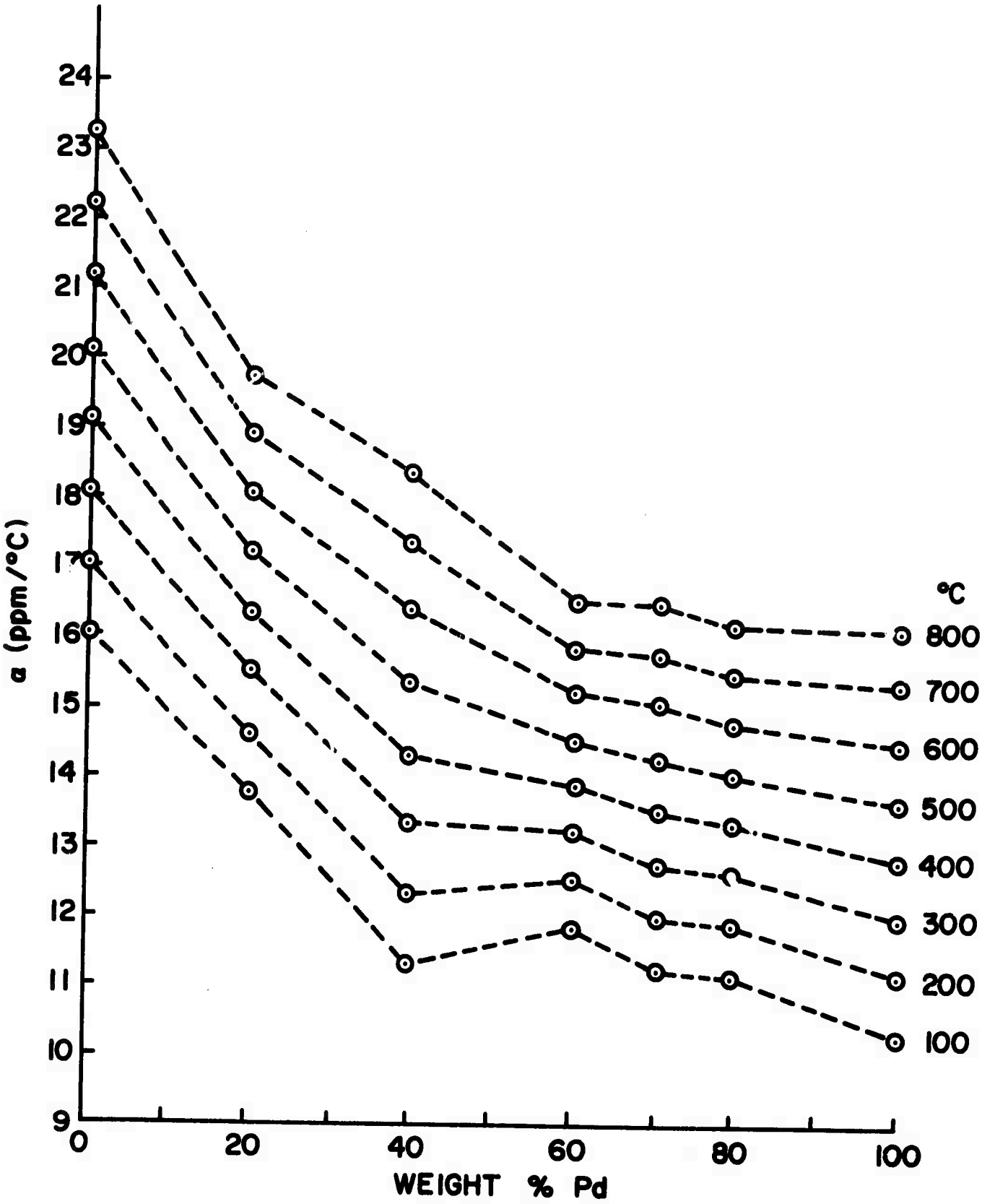

Figure 10. Thermodynamic Coefficient of Linear Thermal Expansion as a Function of Composition in the Silver-Palladium System

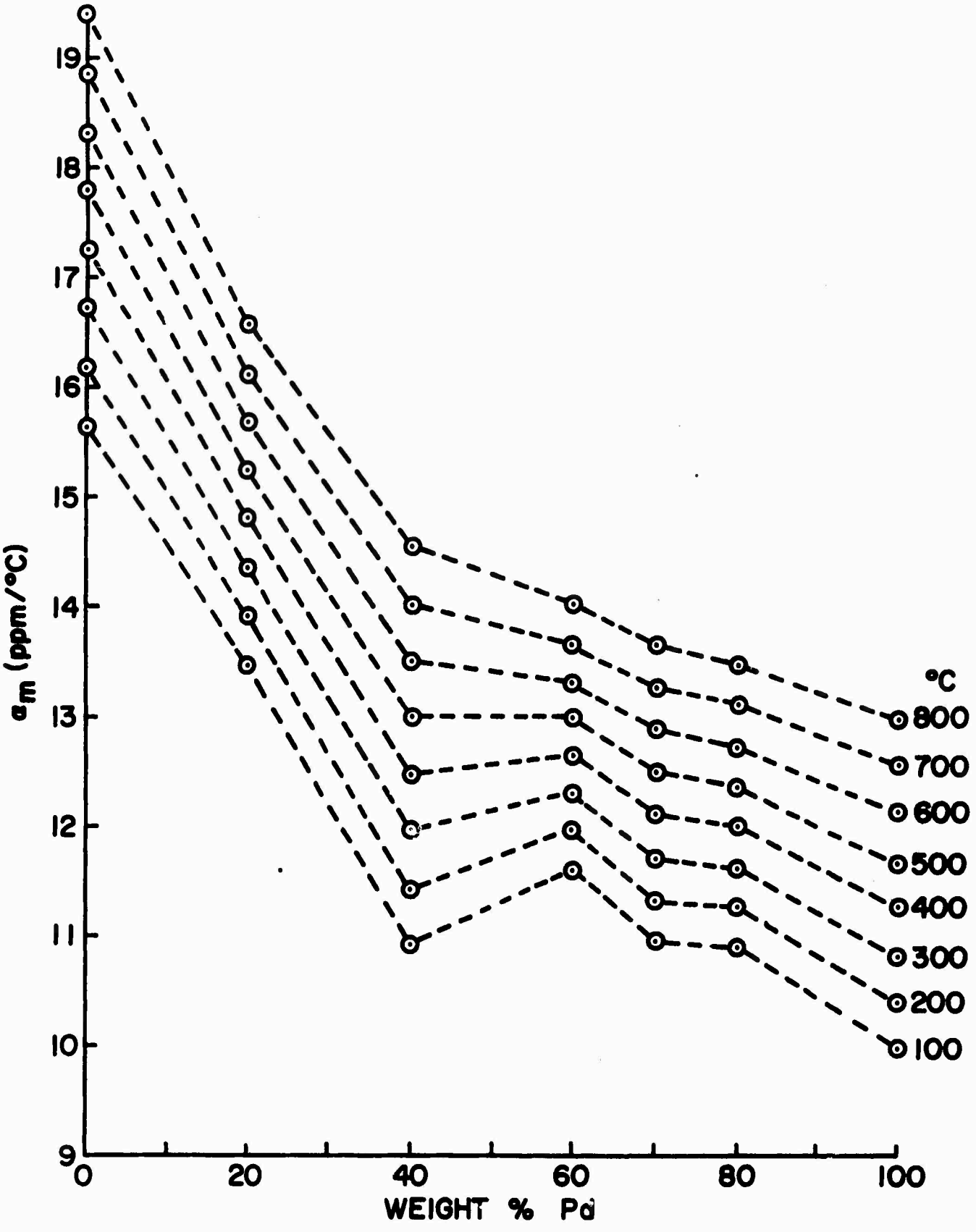

Figure 11. Mean Coefficient of Linear Thermal Expansion as a Function of Composition in the Silver-Palladium System

parent metals; it is apparent from Figs. 10 and 11 that this is a poor approximation. The accepted phase diagram has been questioned by Savitskii and Pravoverov [12] who propose the existance of two Kurnakov phases, Ag_2Pd_3 and AgPd, corresponding to 40% and 46% Pd by weight. The compositional dependance of the thermal expansion from this study in addition to the resistivity, TCR, and mechanical properties [4] are more easily explained on the basis of this more complex phase diagram.

2. Gold-Platinum

The parameters calculated from expansion data over the temperature range 22° -800°C for the various gold-platinum alloys are given in Table IV. Fig. 12 shows the relative expansion of the alloys and Figs. 13 and 14 show the thermodynamic and the mean coefficients of linear thermal expansion at various temperatures. The value of α_m for pure gold from room temperature to 500°C found in this study (13.9) is slightly lower than the literature [11] value (14.2), but the agreement is considered to be satisfactory.

The accepted phase diagram [3] for the gold-platinum system shows a solid solution miscibility gap with a critical point of 1252 ± 1.5°C, 60 ± 0.7 a/o Pt [13]. The solubility limits of the two phase field were found [14] to be 26 and 93 a/o Pt at 727°C. The thermal expansion of a two-phase composite body can be predicted with the equation derived by Turner [15]. In his derivation the average coefficient of the composite is given by

$$\alpha = \frac{\frac{\alpha_1 E_1 W_1}{d_1} + \frac{\alpha_2 E_2 W_2}{d_2}}{\frac{E_1 W_1}{d_1} + \frac{E_2 W_2}{d_2}}$$

Table IV

Calculated Parameters for Thermal Expansion of Gold-Platinum Alloys

$$L = L_o + a(T-22^\circ) + b(T-22^\circ)^2$$

weight % Pt	L_o(in)	a(in/°C)	b(in/°C^2)
0	0.533	6.53×10^{-6}	1.89×10^{-9}
10	0.515	6.03×10^{-6}	1.04×10^{-9}
20	0.539	5.62×10^{-6}	1.50×10^{-9}
25	0.546	5.67×10^{-6}	1.69×10^{-9}
39	0.577	5.90×10^{-6}	1.61×10^{-9}
60	0.491	4.35×10^{-6}	1.47×10^{-9}
70	0.436	3.65×10^{-6}	1.07×10^{-9}
80	0.566	4.29×10^{-6}	1.91×10^{-9}
94	0.545	4.11×10^{-6}	1.50×10^{-9}

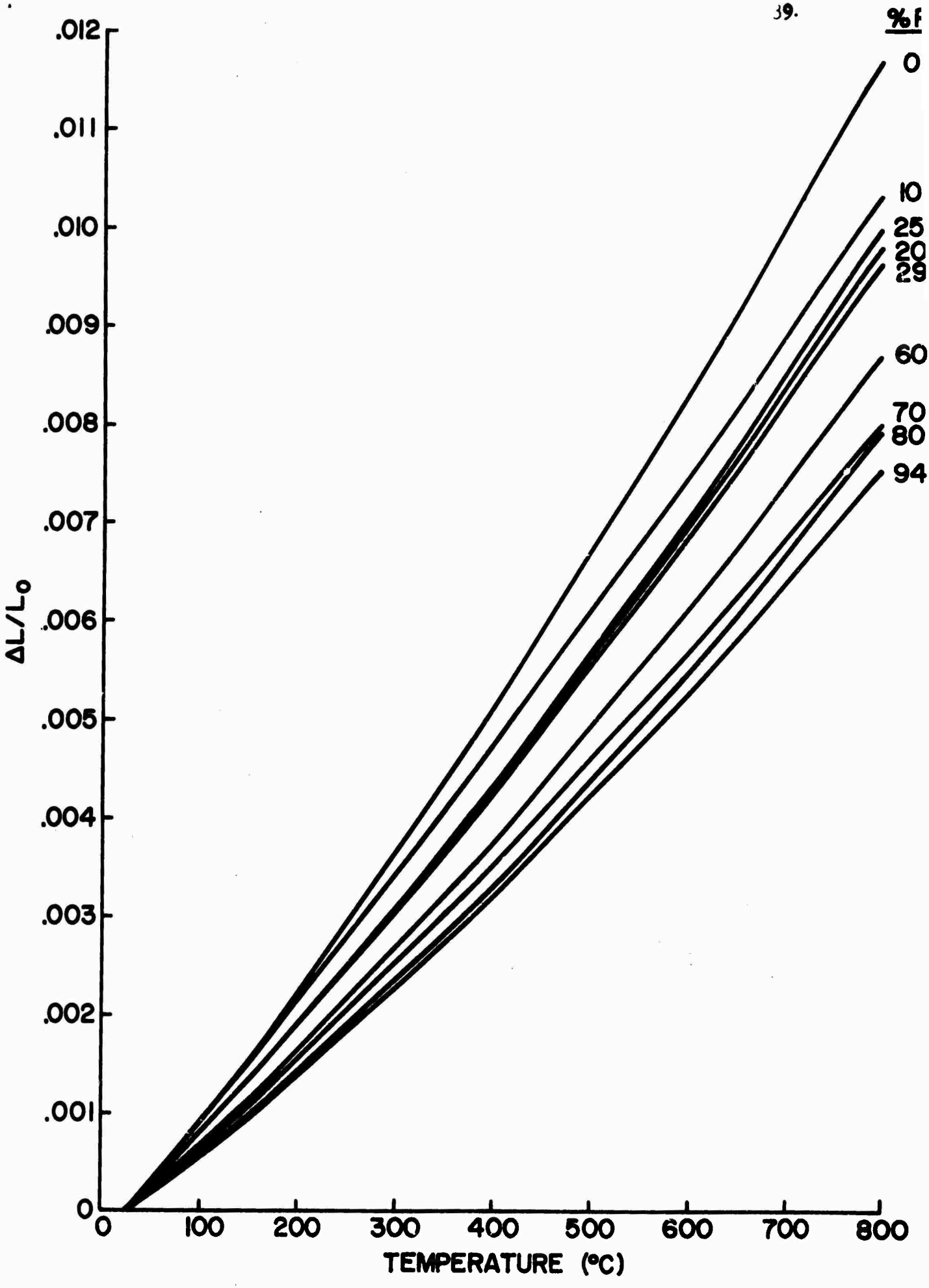

Figure 12. Relative Expansion of Gold-Platinum Alloys

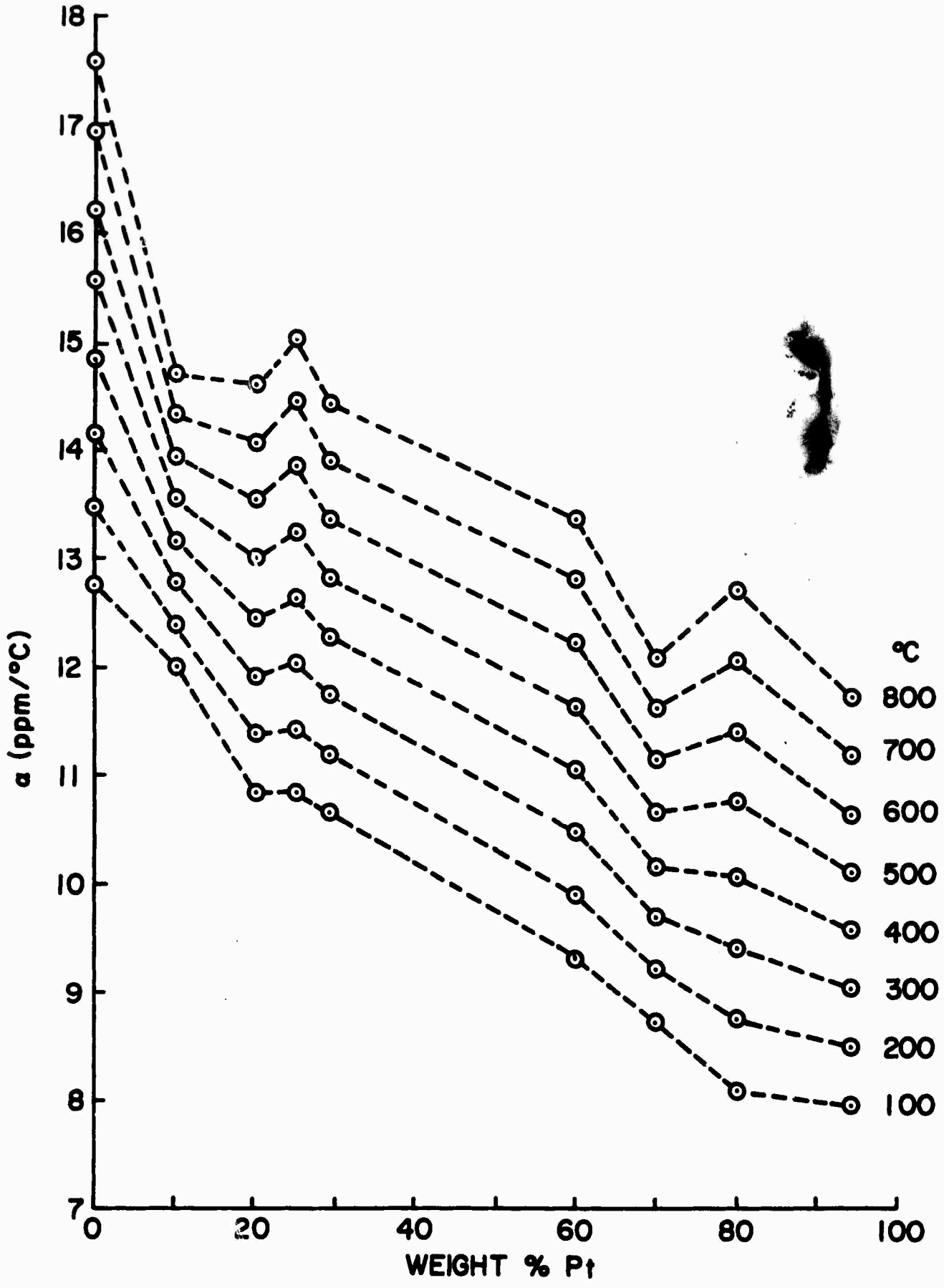

Figure 13. Thermodynamic Coefficient of Linear Thermal Expansion as a Function of Composition in the Gold-Platinum System

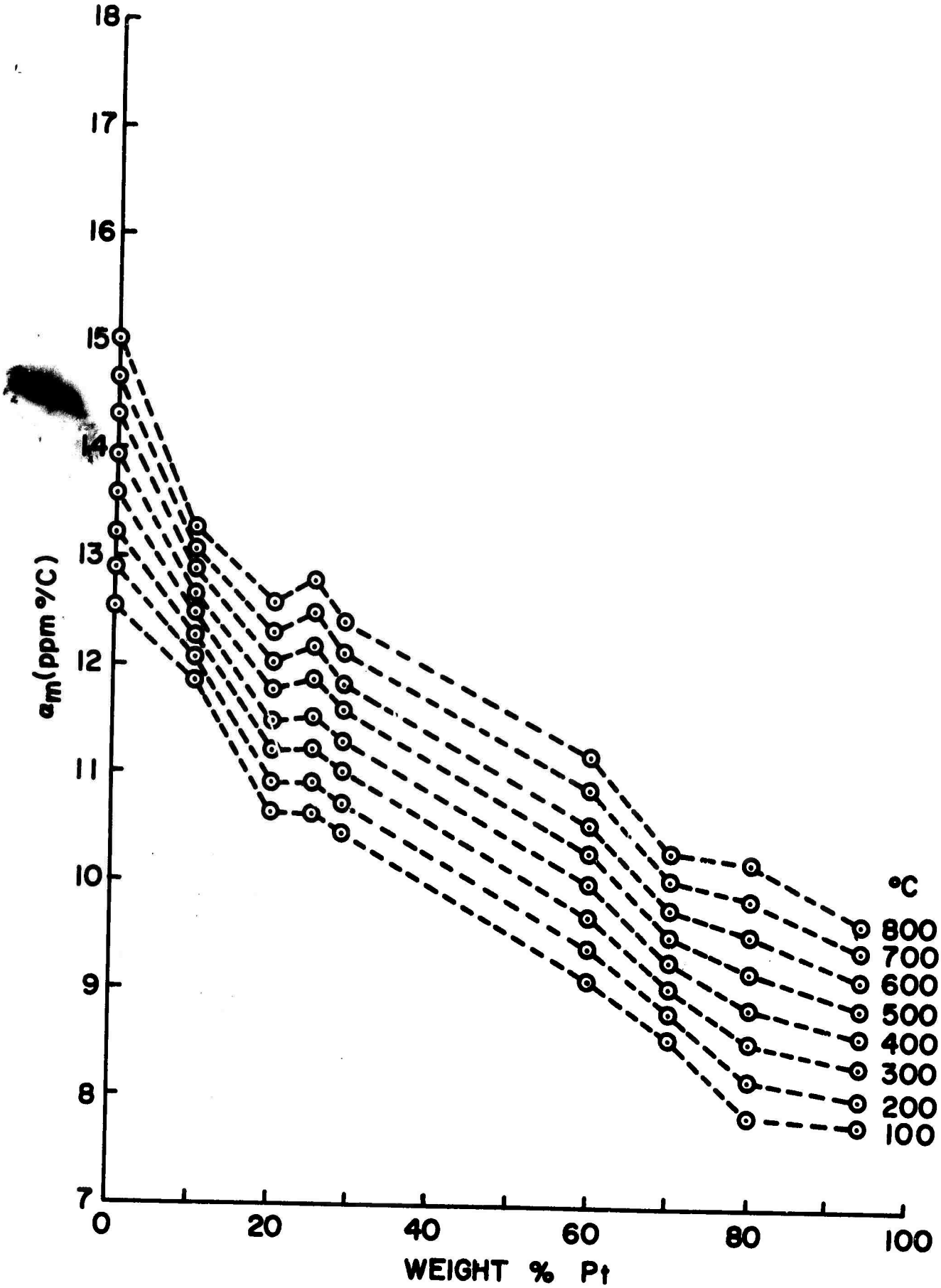

Figure 14. Mean Coefficient of Linear Thermal Expansion as a Function of Composition in the Gold-Platinum System

where α_1 and α_2, E_1 and E_2, W_1 and W_2, and d_1 and d_2 are the coefficients, Young's modulus, weight fraction, and density of the two phases respectively. By taking the 25% and 94% Pd alloys as the two phases and calculating their moduli and densities from those of pure Au and Pt it should be possible to predict the coefficient of linear thermal expansion for any alloy in the two-phase field. The result of this calculation for the mean coefficient from 22° - 500°C is plotted as the solid line in Fig. 15. The agreement with the experimental points is quite good, and serves as corroboration of the two-phase nature of the alloys throughout this temperature range.

The anomaly observed in the coefficients at 20% Pt (Figs. 13 and 14) may be due to a $PtAu_3$ phase, but the stability of this phase is in doubt [16].

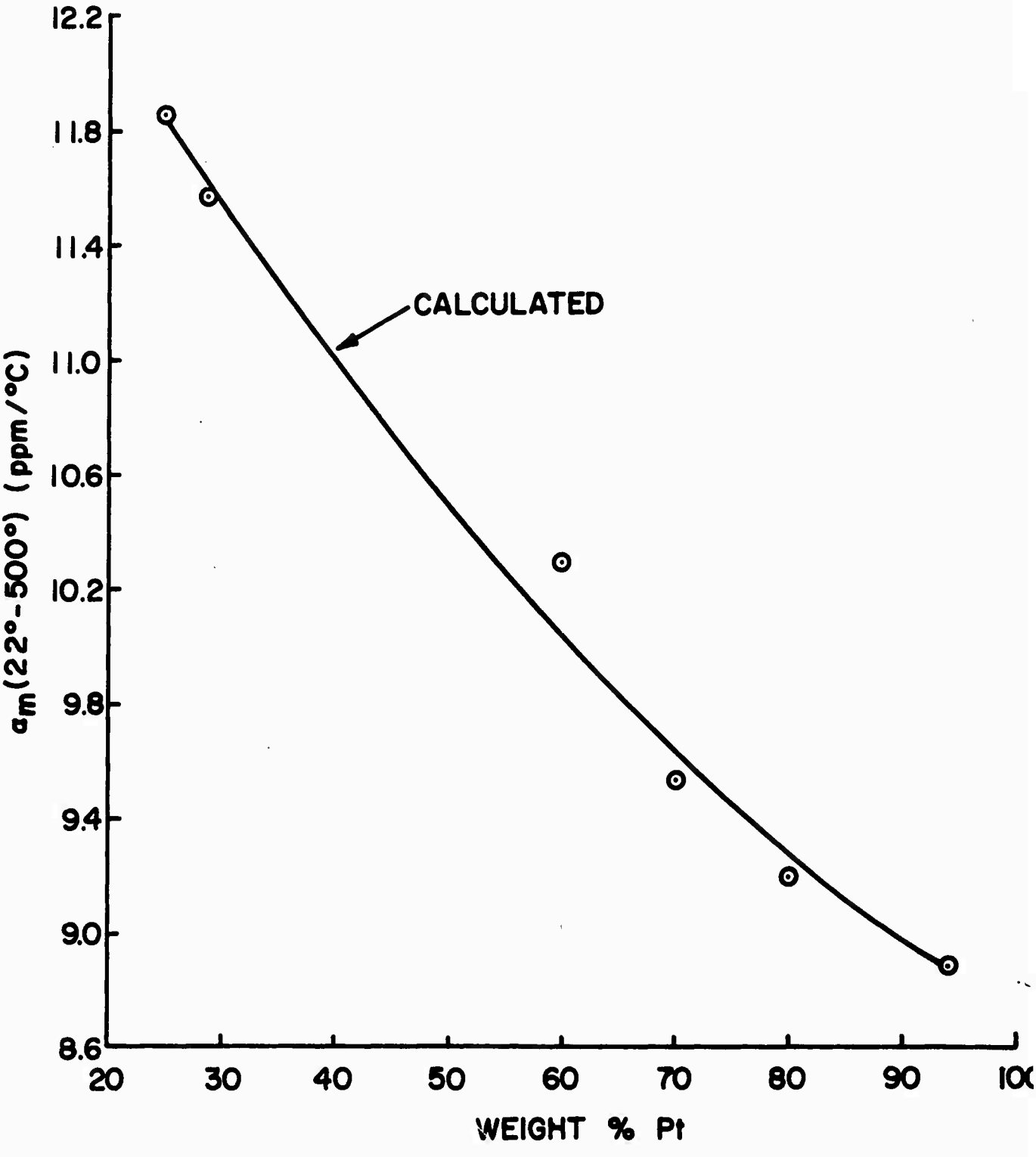

Figure 15. Comparison of Theory and Experiment for the Mean Coefficient of Linear Thermal Expansion from 22° to 500°C in the Two Phase Region of the Gold-Platinum System

IV. SUMMARY AND FUTURE PLANS

The properties of a single contact between RuO_2 particles in the presence of glass have been measured. This is a necessary step in developing a conduction mechanism which relates material properties to electrical behavior. The influence of interfacial forces was shown to be the primary factor in the initial formation of the contact. Several possible models were discussed to explain the resistance and TCR of the contact; the differences in these models suggest experiments to distinguish among them.

The thermal expansion studies of Ag-Pd alloys indicate that there is some sub-solidus structure in the phase diagram for this system; complete solid solution is not compatible with the results. The thermal expansion studies of Au-Pt alloys confirm the existance of the wide two-phase region.

Work directed toward resolving the "TCR Anomaly" and developing models for conduction mechanisms in thick film resistors will continue. In addition to continuing some of the studies described in this report, the following work is planned:

1. Measurements of the contact resistance of RuO_2 powder as a function of both temperature and pressure will be completed.
2. The coefficient of thermal expansion of the glass will be varied by changing the ratios $PbO/B_2O_3/SiO_2$, and the effect on resistivity and TCR of massive glass-RuO_2 samples determined.

3. Substrates with coefficients of thermal expansion differing by more than a factor of ten have been obtained and flame sprayed with a thin coating of alumina so that the resistor-substrate interface will be the same in all cases. The resistance and TCR of resistors printed and fired on these substrates will be measured.
4. Studies of tunneling through thin glass layers on RuO_2 will be initiated.
5. Studies will be initiated in the areas of formulation rheology and screen printing. The purpose of these studies will be to reduce the variations in resistor properties due to these two factors to a small and known level.
6. Studies of resistor and conductor microstructure as a function of material properties and processing conditions will be initiated.

V. REFERENCES

1. R.W. Vest, Semi-annual Technical Report for the Period 7/1/70 - 12/31/70, Purdue Research Foundation, Grant No. DAHC15-70-G7, ARPA Order No. 1642, February 1, 1971.

2. Commercial Products Information Bulletin A-74672, "Method of Test for Wire Peel Adhesion of Soldered Thick Film Conductives to Ceramic Substrates", E.I. DuPont De Nemours and Co., March 1971.

3. M. Hansen,"Constitution of Binary Alloys", McGraw-Hill, New York, 1958.

4. R.F. Vines, "The Platinum Metals and Their Alloys", The International Nickel Company, Inc., New York, 1941.

5. ASTM Method of Test E228-66aT, for Linear Thermal Expansion of Rigid Solids with a Vitreous Silica Dilatometer, 1967 Book of ASTM Standards, Part 31

6. N.C. Miller and G.A. Shirn, Solid State Tech., 10, 28 (1967).

7. R. Holm and E. Holm, "Electric Contacts", p. 123, Springer-Verlag, Berlin, 1967.

8. J.G. Simmons, J. Appl. Phys., 35, 2655 (1964).

9. ibid, 34, 1793 (1963).

10. F.W. Schmidlin, J. Appl. Phys., 37, 2823 (1966).

11. "Handbook of Tables for Applied Engineering Science", R.E. Boly and G.L. Tuve, Eds., Chemical Rubber Co., Cleveland, Ohio, 1970.

12. E.M. Savitskii and N.L. Pravoverov, Russ. J. Inorg. Chem., 6, 253 (1961).

13. A. Munster and K. Sagel, Z. Physik. Chem. (Frankfurt), 23, 415 (1960).

14. J.L. Meijering, Phys. Chem. Solids, 18, 267 (1961).

15. P.S. Turner, J. Res. NBS, 37, 239 (1946).

16. V.V. Sanadze, Proc. Acad. Sci. USSR, Chem. Sect., 140, 889 (1961).